Makara Journal of Science

Volume 27
Issue 3 *September*

Article 9

9-25-2023

Antibacterial Testing on Silver/Zinc Oxide Nanoparticles/ Organoclay Reinforced Chitosan Biocomposites

Lisna Junaeni Muiz
Department of Chemistry, Faculty of Mathematics and Natural Sciences, Universitas Indonesia, Depok 16424, Indonesia

Ariadne Lakshmidevi Juwono
Department of Physics, Faculty of Mathematics and Natural Sciences, Universitas Indonesia, Depok 16424, Indonesia

Zulkarnaen Paputungan
Dipartemento Chimica Industriale "Toso Montanari", Università di Bologna, Bologna 40136, Italy

Yuni Krisyuningsih Krisnandi
Department of Chemistry, Faculty of Mathematics and Natural Sciences, Universitas Indonesia, Depok 16424, Indonesia, yuni.krisnandi@sci.ui.ac.id

Makara Journal of Science, 27/3 (2023), 235–246
doi: 10.7454/mss.v27i3.2114

Antibacterial Testing on Silver/Zinc Oxide Nanoparticles/Organoclay Reinforced Chitosan Biocomposites

Lisna Junaeni Muiz[1], Ariadne Lakshmidevi Juwono[2], Zulkarnaen Paputungan[3], and Yuni Krisyuningsih Krisnandi[1,4 *]

1. Department of Chemistry, Faculty of Mathematics and Natural Sciences, Universitas Indonesia, Depok 16424, Indonesia
2. Department of Physics, Faculty of Mathematics and Natural Sciences, Universitas Indonesia, Depok 16424, Indonesia
3. Dipartemento Chimica Industriale "Toso Montanari", Università di Bologna, Bologna 40136, Italy
4. Solid Inorganic Framework laboratory, Department of Chemistry, Faculty of Mathematics and Natural Science, Universitas Indonesia, Depok 16424, Indonesia

E-mail: yuni.krisnandi@sci.ui.ac.id

Received May 17, 2023 | Accepted July 12, 2023

Abstract

Herein, bionanocomposites of chitosan (CS)/silver nanoparticle/organoclay/zinc oxide nanoparticle (CS/Ag/OC/ZnO) were prepared for antibacterial food packaging. This study examines the time variation in the AgNP synthesis method by comparing local (74-85% deacetylated) and commercial chitosan (75%-85% deacetylated) as a reducing and capping agent and seeks to reconstruct the optimum ratio formulations of AgNPs and ZnONPs in bionanocomposites for food packaging. The results reveal that the synthesis of AgNPs was successfully carried out using a local chitosan solution as a reducing and capping agent. The CS/Ag/OC/ZnO films exhibit structural, mechanical, and optical properties suitable for food packaging and antibacterial activity on *Staphylococcus aureus* and *Escherichia coli.* The relative inhibition zone increased with increasing numbers of AgNPs and ZnONPs. The inhibition zone values indicated that *E. coli* and *S. aureus* bacteria were sensitive to the film, namely 12.5 ± 1.5 mm, and 16 ± 0.0 mm, respectively.

Keywords: chitosan, organoclay, silver, zinc oxide

Introduction

The development of biodegradable antibacterial food packaging is a crucial aspect of food preservation. It offers several benefits, including protecting food from environmental decay and its environmentally friendly nature, which can be attributed to its ability to decompose naturally with ease.Antibacterial agents have been widely used by many researchers as additives added to the polymer matrix, includingboth natural and synthetic antibacterial agents [1].

In particular, silver nanoparticles (AgNPs) have been of great interest to researchers due to their antibacterial properties [2]. Zinc oxide nanoparticles (ZnONPs) also serve as a viable alternative owing to its diverse morphology, reactivity, strong antibacterial properties, and ability to interact with cells [3]. Moreover, due to the fact that AgNPs and ZnONPs have low toxicity, they are safe to be used as additives in food packaging [1].

The synthesis method determines the properties of the resulting nanoparticles. Synthesis methods are grouped into chemical synthesis and green synthesis. Green synthesis is expected to reduce the impact of chemicals on the environment. Extracts from bio-organisms can act as both reducing and capping agents in the synthesis of AgNPs [4]. Herein, chitosan (CS) was chosen as a reducing and capping agent in the synthesis of AgNPs due to the presence of hydroxyl groups and amine groups in its local CS. These groups can be activated to reduce silver ions [4]. There are many manufacturers who produce commercial CS. The author aimed to investigate the ability of commercial CS as a reducing and capping agent compared to local CS with the same degree of deacetylation.

Zain *et al.* [5] studied the effect of CS solution concentration and silver nitrate concentration on the particle size of AgNPs using microwave heating and found that increasing nitrate concentrations and decreasing

CS concentrations increases the particle size of AgNPs. Wongpreecha *et al.* [6] investigated the effects associated with temperature and pressure inputs on particle formation in a systematic manner. The results of the synthesis of AgNPs/CS exhibit antibacterial activity against *E. coli* and *S. aureus*. Fetouh *et al.* [7] used a different duration contact with CS solution or reaction time ranging from 1 to 16 h. The results of the study found that sample 2 h showed the most constant inhibition efficiency. Further, Affes *et al*. [8] studied the effect of variations in the molecular weight of CS on the production of AgNPs and CS/AgNPs nanocomposite films, attempting to find potential applications of this effect in novel alternative food packaging applications.The results showed that the characteristics of CS remarkably influenced the stabilization as well as the physicochemical and biological properties of AgNPs. Therefore, the conclusion is that the use of suitable CS samples can control the morphology and size of the AgNPs.However, because these CS/AgNPs nanocomposite films have low tensile strength. Therefore, in this study, the weak mechanical properties of CS-based films could be improved by adding fillers to the matrix.

Gabriel *et al*. [9] studied the photochemical synthesis of AgNPs on CS/montmorillonite (CS/MMT) nanocomposite films using different molar masses and deacetylation degrees of CS, as well as those modified with diethyl aminoethyl (DEAE) and dodecyl groups. Their findings showed the growth of *E. coli* and *B. subtilis* could be inhibited by all the nanocomposite-AgNPs films. Zahedi *et al.* [10] studied the effect of variations of ZnONPs (1, 2, 3, and 4 wt%) on the physical and mechanical properties of the MMT/ZnONPs hybrid carboxymethyl cellulose (CMC) nanocomposite. The results showed that the ability to pass gas and water vapor of the films decreased by approximately 53%, whereas the moisture content, density, temperature resistance of the glass, and tensile stress increased with an increasing number of NPs. Thus, the ability of MMT as a filler increases by adding organic sites to the clay structure to form organoclay (OC).

To our knowledge, this study is the first report to evaluate the comparative effect of local and commercial CS as reducing and capping agents on the resulting AgNPs. In addition, the combined effect of AgNPs and ZnONPs on the physical and antibacterial properties of CS/Ag/OC/ZnO films was investigated. The study hypothesis is that local CS can act as a reducing and capping agent in the synthesis of AgNPs. Moreover, the optimum composition of AgNPs and ZnONPs in the CS/Ag/OC/ZnO nanocomposite produces the best properties of the composites as antibacterial films.

Materials and Methods

Materials. The materials used in this study were chemicals obtained from Merck, including CS (relatively low molecular weight, 50–190 kDa), with a degree of deacetylation of 75%–85%, silver nitrate, zinc acetate dihydrate, hexadecyltrimethylammonium bromide, sodium hydroxide, acetate acid (99% v/v), and ethanol (99% v/v). Other chemicals were natural clay from Pacitan, Indonesia (CV. Adista Makmur Santosa) and local CS (CV. Bio Chitosan Indonesia).

Preparation of materials. CS was prepared via the deacetylation reaction of 10 g of local CS added to 150 mL of 60% NaOH (w/v), then heated at a temperature of 120 °C for two hours using a reflux set. The result was washed, filtered, and dried at 60 °C. The commercial CS was used as received.

OC was prepared from Na-MMT that was the result of the purification and uniformization of cations from natural clay. Five grams of Na-MMT was dispersed in 75 mL of doubly distilled water and stirred for 1 hour. In another beaker, the surfactant HDTMABr 1 CEC was dissolved in 25 mL of doubly distilled water. After 1 hour of stirring, HDTMABr surfactant was added slowly and again stirred for 1 hour at 60 °C; then the mixture was sonicated for 3 minutes. Next, the mixture was washed several times until it was free from bromide ions. The precipitate was then centrifuged and dried at 70 °C.

ZnONPs were synthesized according to Magesh *et al*. [12] with slight modifications. A CS solution (1%, w/v) was stirred for 30 minutes at 50 °C. Zinc acetate (0.2 M) was added to the solution with 1500 rpm stirring, and then NaOH (0.1 M) was added dropwise to pH 12 to form a precipitate. The white precipitate formed was left for 24 hours, then washed and dried at 70 °C.

Preparation of CS/Ag based films. The synthesis of CS/Ag nanocomposites was adopted from the method of Kalaivani *et al*. [13] with slight modifications. A total of 100 mL of local CS solution (1% w/v) was stirred and heated at 90 °C. The amounts of 3 mL of $AgNO_3$ (0.1 M) and 0.5 mL of NaOH (0.1 M) were mixed with the CS solution and continuously stirred for 30, 60, and 90 minutes at a temperature of 90 °C. The same treatment was carried out using commercial CS as a comparison to local CS.

In another beaker, 0.05 g of OC was stirred into 10 mL of 1% (v/v) acetic acid for 24 hours. The amount of 50 mL of CS/Ag nanocomposite was mixed with the OC suspension and stirred for 4 hours. The mixture was then added by 0.025 g of ZnONPs, stirred for 2 hours and sonicated for 15 minutes. After that, the suspension was poured into a petri dish (15 cm) and dried at 65 °C. The film was peeled from the petri dish using a 3 M NaOH solution, washed, and allowed to dry naturally. The composition of AgNPs and ZnONPs in the CS matrix was then varied with a mass ratio of 5%, 7%, and 9%

Characterization of films. The functional groups of CS/Ag-based films were identified using the attenuated total reflection (ATR) method via Fourier transform infrared spectroscopy (Bruker Alpha, ATR platinum Diamond). The measurements were conducted of 128 scans in 4000–400 cm^{-1}. X-ray diffraction (XRD) diffractogram analysis was performed to identify the crystalline phase and film crystallinity (PANalytical X'Pert PRO 2318). XRD analysis was carried out with Cu Kα radiation (λ = 1.54 Å) at 40 kV, a current of 30 mA, a time per step of 0.02, with an angle of 2θ between 3˚–90˚ and nickel as the filter metal.

The X-ray fluorescence (XRF) (PANalytical εpsilonl) method was used qualitatively and semi quantitatively to determine the elemental composition contained in the films. The films sample (2 × 2 cm) was excited with x-ray that caused fluorescence. The filter used was Ag (silver) with a current of 1.5 mA and a voltage of 50 kV. The measurement method was Energy Dispersive (ED) XRF.

UV–Vis spectrophotometry. A UV–Vis spectrophotometer (T92+, PG Instruments) was used to characterize the AgNPs synthesized. The formation of AgNPs can be analyzed using the UV–Vis spectrum through the absorption peaks of the surface plasmon resonance (SPR) phenomena on metals. The absorbance of AgNPs colloids was measured at a wavelength of 200–800 nm [13].

A UV–Vis spectrophotometer was also used to determine the absorbance of CS-based plastics in the ultraviolet and visible wavelength regions and to evaluate the transparency properties of films. Transmittance of a 2 × 2 cm sized film was measured at a wavelength range of 200–800 nm [14].

Morphological analysis. CS/Ag-based films were observed by transmission electron microscope (FEI Tecnai G2 SuperTwin TEM) to determine the morphology of the AgNPs, ZnONPs (see figure in supplement data), and OC formed as well as to map their distribution in the CS matrix. The film samples were first powdered using liquid N_2. The powdered samples were mixed in ethanol using ultrasonic for five minutes. The sample was dripped onto the Cu grid surface, dried at room temperature, and measured at 120 kVA power [15].

Mechanical properties of films. The mechanical properties of CS/Ag-based films were assessed using the ASTM D882 standard. The films (10 × 100 mm) were tested using a Shimadzu AGS 10 kN UTM (Load Cell 200 N) with a speed of 10 mm/minute, grip distance of 50 mm, temperature of 22.9 °C, and relative humidity of 59.6% to obtain percent elongation and tensile strength. Measurements were carried out with five repetitions for one sample [16].

Water Solubility (WS) of films. The film's solvent resistance to water was tested by immersing the film sample (10 mm × 50 mm) in distilled water for 24 hours, then drying it at 60 °C. Before and after immersion, the thin layer was weighed. The solubility properties of thin films in water were determined by using Equation 1:

$$WS\ (\%) = W_1\text{-}W_2/W_1 \times 100 \quad (1)$$

where W_2 is the weight of the film after it soaked for 24 hours in solvent and W_1 is the weight of the initial film conditioned at 60 °C for 12 hours to completely remove moisture [17].

Water Vapor Transmittance Rate (WVTR) of films. The WVTR was calculated by the gravimetric method. The film was cut into the surface area of the bottle mouth. The bottle was filled with distilled water as much as half of the volume of the bottle. Then the film was attached to the mouth of the bottle with tape. The mass of the bottles covered with film was weighed before and after being heated at 40 °C for 24 hours. WVTR (g/ (m^2.h)) was calculated by determining the amount of water vapor that passed through the material being tested per unit area (m^2) per unit time (24 hours/day) at a certain temperature and relative humidity, according to Equation 2:

$$WVTR = (W_1\text{-}W_2)/(A.t) \quad (2)$$

where W_2 is the weight of the film after being heated at 40 °C for 24 hours, W_1 is the initial layer weight, A is the inner surface area of the bottle, and t is the heating time [18].

Antibacterial activity of films. The agar diffusion method was used for antibacterial testing at the Microbiology Department, Faculty of Medicine, University of Indonesia. This test uses *S. aureus* ATCC 25.922 (Gram-positive bacteria) and *E. coli* ATCC 25.923 (Gram-negative bacteria), with a concentration of 0.5 McFarland. The antibiotics used on *S. aureus* and *E. coli* bacteria are Vancomycin and Erythromycin, respectively [19]. This method is accurate for testing antibacterial films because the film is exposed to the bacteria in the agar, so it is gradually deactivated.

Results and Discussion

Physicochemical properties of colloid. The film fabricated in this study was a CS/Ag nanocomposite–based film. CS/Ag nanocomposite was a colloidal product synthesized by AgNPs using CS as a reducing agent and capping agent. The CS consisted of local and commercial CS. The NH_2 and OH groups in the β (1–4) D-glucosamine units of CS can bind to the resulting Ag^+ ions [20].

Figures 1 shows comparative photos of the colloidal color synthesized by CS/Ag nanocomposite between

local and commercial CS at 30, 60, and 90 minutes of heating time. The characteristic color of AgNPs is golden yellow [13]. Longer heating times produced a corresponding increase in the concentration of colloidal color, i.e., brownish yellow. There is a difference in color between the results of synthesis using local CS and commercial CS. Namely, the colloid color synthesized by CS/Ag nanocomposite using local CS (Figure 1a) shows a transparent solution, whereas that using commercial CS (Figure 1b) shows a cloudy solution. This is because of the difference in turbidity, which may be caused by agglomerated AgNPs, whereas clear/transparent colloids do not experience agglomeration because CS functions as a strong capping agent.

This colloid was analyzed using a UV-Vis spectrophotometer to show the presence of surface plasmon resonance absorption (SPR). SPR is an optical property of metal nanostructures resulting from interaction with light, which causes coherent collective oscillation of the free electron conduction band [21]. The UV-Vis spectra showed SPR at a wavelength of 410 nm (Figure 2). This SPR only appeared in the synthesized CS/Ag nanocomposite sample with a heating time of 30 minutes because using a longer heating time causes the color of the colloid to become more concentrated, so it is necessary to dilute it (Figure 3).

Figure 2 illustrates that the SPR on local CS is higher than that on commercial CS. This suggests that the number of AgNPs formed in colloids synthesized with local CS is greater than that in colloids synthesized with commercial CS. The high SPR of the synthesized AgNPs using local CS implies that a collective oscillation is generated by the optical properties of the AgNP structure, which results from interaction with light. These oscillations are observed to be greater than those obtained from the results of the synthesis of AgNPs using commercial CS. Therefore, the colloid used for film fabrication is the result of the synthesis of CS/Ag nanoparticles with local CS as a reducing agent and capping agent with a heating time of 30 minutes.

Figure 3 displays the UV–Vis spectra of the colloid-synthesized CS/Ag nanocomposite (dilution 2 times) with heating times of 30, 60, and 90 minutes. The synthesis results revealed that the longer the heating time, the more concentrated the yellow color in the solution and the higher the absorption in the UV–Vis spectrum. The absorption of the synthesized AgNPs using local CS was 2.3, whereas the absorption of the synthesized AgNPs using commercial CS was 1.6. This high absorption is attributable to the presence of a dense color, which is in turn attributable to the long heating time in the synthesis process, and not a result of the SPR phenomenon. This is because this dilution can reduce the AgNP collective oscillations that cause invalid SPR values [11, 22]. Thus, the AgNPs colloid used for fabricating CS-based films is colloid without dilution. Another reason is that the ability of CS to form films will decrease if the colloid used is the result of dilution because there is a decrease in the concentration of CS in the film. Film formation is considered to be the most important property of CS [22].

Transparency properties of films. The physicochemical properties of films in this study are transparency, functional groups, crystallinity, morphology, mechanical strength, solubility, and WVTR. Transparency can be demonstrated by the visual appearance of the transparency and light transmission spectra (Figures 4). CS film visual transparency (Figure 4a) displays a clear and transparent film, whereas CS/Ag/OC/ZnO film visual transparency (Figure 4b) exhibits a golden yellow color and is less transparent. This is because the color of the fabricated film follows the colloidal color of the AgNPs.

The transparency properties of the film are also supported by the light transmission spectra (Figure 4c), which shows that the transmittance value of the CS film is higher than that of the CS/Ag/OC/ZnO film. This indicates that the CS film is more transparent than the CS/Ag/OC/ZnO film. Thus, the presence of AgNP, ZnONP, and organoclay caused a decrease in the transparent properties of the film.

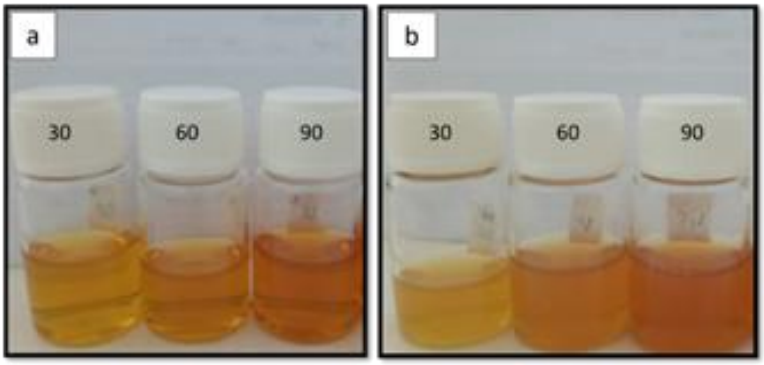

Figure 1. Colloid Synthesized by CS/Ag Nanocomposites with Variations in Heating Time of 30, 60, and 90 Minutes (a: Local CS, b: Commercial CS)

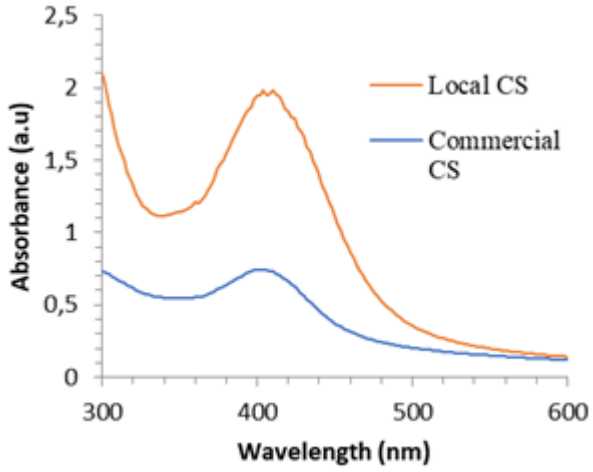

Figure 2. UV-Vis Spectra of Colloid Synthesized CS/Ag Nanocomposites with a Heating Time of 30 Minutes using Local and Commercial CSs

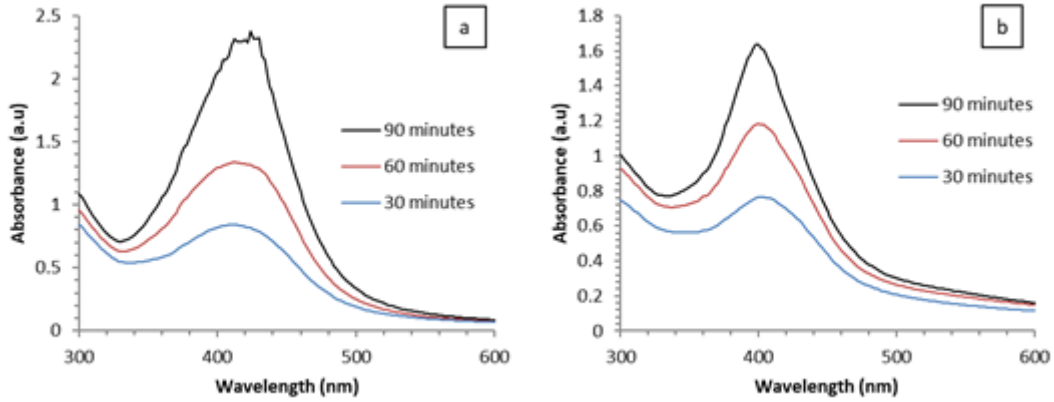

Figure 3. UV–Vis Spectra of Colloid-synthesized CS/Ag Nanocomposite (Dilution 2 Times) with Heating Times of 30, 60, and 90 Minutes (a: Local CS, b: Commercial CS)

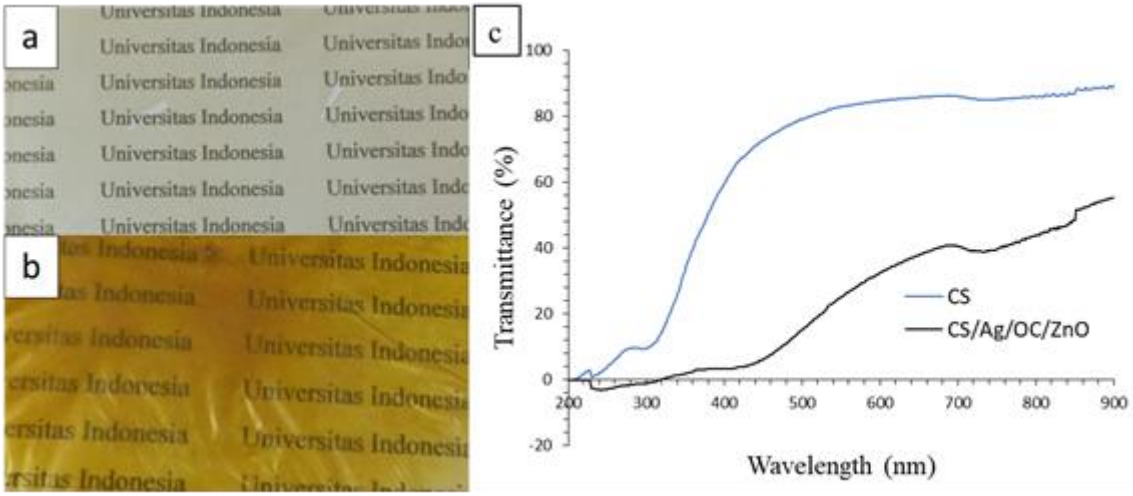

Figure 4. CS Film Visual Transparency (a), CS/Ag/OC/ZnO Film (b), and Light Transmission Spectra of the CS Film and CS/Ag/OC/ZnO Film (c)

ATR–FTIR analyses of films. Intermolecular structural interactions between CS, AgNP, ZnONP, and OC on films were characterized using ATR–FTIR. Figure 5 is the spectrum of neat CS films and CS/Ag/OC/ZnO films. The band width between 3500 and 3000 cm^{-1} is an interpretation of the stretching vibration of the –OH group which often overlaps with the N–H bond of the amino group [23].

The peaks at approximately 2910 and 2876 cm^{-1} are associated with $–CH_2$ and –CH stretching vibrations. The peak at 1658 cm^{-1} is related to the bending vibration of carbonyl and imide groups, whereas the peak at 1410 cm^{-1} is associated with C=O symmetric, and the peak at 1026 cm^{-1} is associated with the C–C stretching group of CS. The peak patterns of the CS/Ag/OC/ZnO CS films do not show a clear shift in wavelength, suggesting a lack of chemical bonding between AgNP, ZnONP, and OC and CS in the CS/Ag/OC/ZnO nanocomposite film. Thus, they only bind physically, and the CS structure does not change after the addition of AgNP, ZnONP, or OC. The small change in peak intensity can be attributed to the non-covalent interactions and hydrogen bonding among the polymers. These results are in parallel with prior research [23].

XRD analyses of films. XRD studies for neat CS film and CS/Ag/OC/ZnO film are illustrated in Figure 6. The XRD diffraction peak of neat CS film at 2θ = 21,10° (202) (denoted as *) [24] decreases the intensity of the XRD diffraction peaks of the CS/Ag/OC/ZnO film. The XRD diffraction peak of OC is located at a 2θ of 22,65° (005) (JCPDS-ICDD number 29-1498) [25, 26]. The XRD patterns from the synthesized AgNPs show the XRD diffraction peaks from AgNPs at a 2θ of 39.60°, 43.50°, and 63.18°. This corresponds to the card number JCPDS-ICDD 04-0783 and is along (111), (200), and (220) Bragg Reflection planes. The synthesized Ag NPs composites contained Ag^+ (Ag_2O) and Ag^{3+}(AgO). The XRD diffraction peak of Ag_2O is at a 2θ of 48.67° (JCPDS file No. 42-0874), whereas that of AgO appears at a 2θ of 35.99° (JCPDS file No. 84-1108). The mechanism of AgNP synthesis is that silver ions are adsorbed on the CS surface, and the Ag^+ complex is incorporated into the NP before the reduction of AgNP. The presence of Ag^{3+} is related to two processes: first, Ag^+ is oxidized to Ag^{3+}, and second, Ag^{3+} is protected in NP [27]. Figures 6 also displays the XRD diffraction peaks of ZnONP at a 2θ of 26.70°, 47.74°, 56.80°, and 66.28° (JCPDS number 361451) corresponding to (002), (101), (110), and (103) Bragg reflection planes, respectively.

Physical properties of films. The CS film and CS/Ag/OC/ZnO films mentioned include WS, WVTR, strength, and elongation (Table 1). A crucial parameter of biopolymer-based packaging films is WS, which satisfies the requirement of maintaining moisture inside the product and the stability of the packaging [17].

The WS value increased from 2.43 ± 0.01% to 5.03 ± 0.49%. Strong hydrophilic properties are one of the main challenges faced by CS-based materials. Its high polarity is due to the several hydroxyl groups in CS. When OC, AgNP, and ZnONP were added, the water absorption increased to 5.03 ± 0.49%. This is due to the hydrophilic nature of OC, which makes the composite film more soluble in water [25]. Another reason is that nanoparticles can disrupt the crystal structure of CS, increasing the WS of the films [26].

The WVTR values of the films were reduced by 85% after the addition of OC, AgNP, and ZnONP. This can be attributed to the nanoparticles being able to block the pores of the film, causing a remarkable increase in the moisture and water resistance of the CS film. The WVTR value shows the film stability and ability to prevent microbial degradation from stored food. Many reports indicate that nanoparticles on the polymer matrix play a

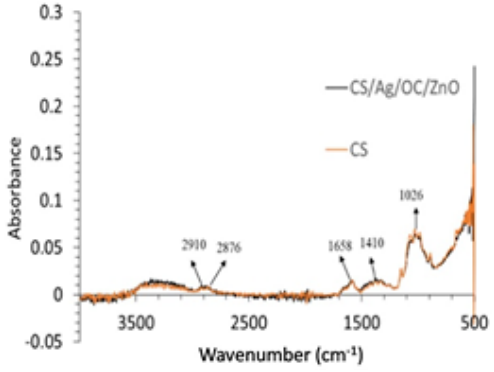

Figure 5. ATR–FTIR Spectra of the CS Film and CS/Ag/OC/ZnO Film

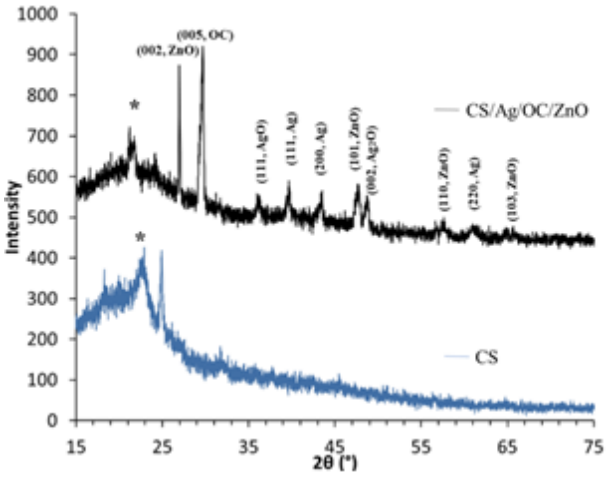

Figure 6. XRD Patterns of the CS Film and CS/Ag/OC/ZnO Film

major role in the reduction of WVTR films [27]. For instance, Saha *et al.* [28] reported that with an increase in the concentration of nanoclay, the WVTR of montmorillonite-loaded cellulose acetate/polyethylene glycol films decreased substantially.

Table 1 shows the physical properties of CS film and CS/Ag/OC/ZnO films. The thickness of the CS film was 0.024 ± 0.004 mm. After the addition of OC, AgNP, and ZnONP, however, an increase was observed in the thickness of the composite films. The tensile strength (TS) and elongation at break (EAB) of the CS film were 48.38 ± 7.24 MPa and 2.90 ± 0.36%, respectively. After the addition of OC, AgNP, and ZnONP, the TS of the composite films increased to 79.73 ± 3.65 MPa, and the EAB values decreased to 2.01 ± 0.56%. Changes in mechanical properties are the main reasons for the strong interaction between CS as a film matrix and OC, AgNP, and ZnONP as fillers that are beneficial for CS/Ag/OC/ZnO film compatibility [29].

Morphology of films. The morphology of CS/Ag/OC/ZnO film was characterized by TEM (Figures 6c and 6d). Figure 6d is an image magnified three times in the selected area from Figure 6c. Spherical images interpret AgNp with diameters within a range of 10–60 nm (Figure 6a). This is in parallel with Kalaivani *et al.*'s [13] research on the synthesis of Ag/CS nanocomposites. The ZnONP TEM image displays the shape of the nanoleafs, and ZnO nanoleafs serve as a step in the mechanism of formation of ZnO nanoflowers [30].

The lines indicated by arrows in Figure 6d represent OC, which exhibits a layered structure. Some OC structures are exfoliated, and others are intercalated. The distance between layers in the intercalated OC layer is approximately 3–10 nm, making it possible for AgNPs or ZnONP to enter the interlayer gallery. Although the distance between layers in the exfoliated OC structure cannot be determined because of the random structure, the thickness of the OC layer can be calculated, and it is determined to be approximately 1 nm. The presence of this intercalation and exfoliation structure serves to increase the mechanical value of CS-based bionanocomposite thin films [31]. The result is in good agreement with the data from the mechanical test results in Table 1, where the value of 79.73 MPa is a moderate TS value for CS-based plastics, which is typically within the range of 10–100 MPa [32].

Table 1. The Physical Properties of CS and CS/Ag/OC/ZnO Films

Film	WS (%)	WVTR (g/m^2h)	Thickness (mm)	Tensile Strength (MPa)	Elongation at break (%)
CS	2.43 ± 0.01	0.28 ± 0.03	0.024 ± 0.004	48.38 ± 7.24	2.90 ± 0.36
CS/Ag/OC/ZnO	5.03 ± 0.49	0.24 ± 0.02	0.038 ± 0.003	79.73 ± 3.65	2.01 ± 0.56

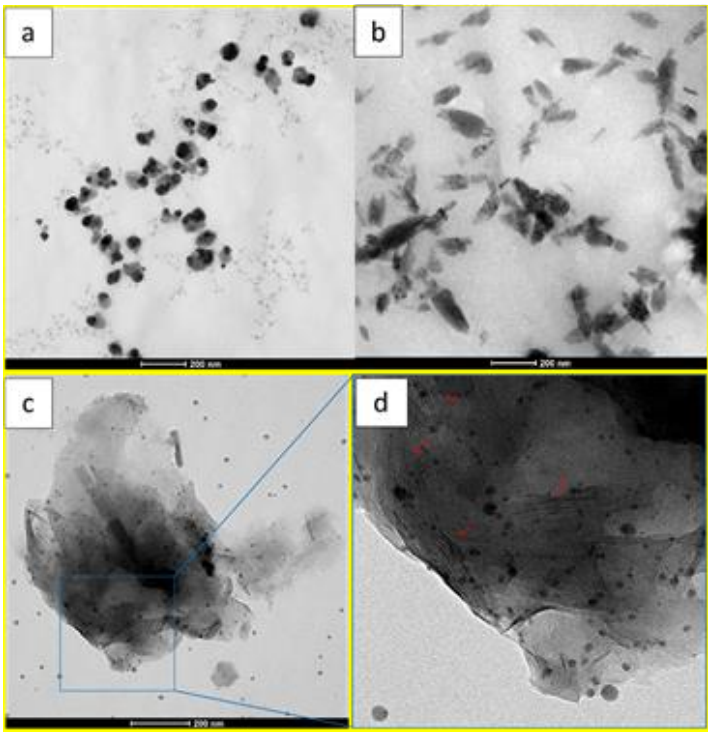

Figure 6. TEM Images of the CS/Ag Nanocomposite (a), ZnONP (b), and CS/Ag/OC/ZnO Film (c and d)

Study of AgNP and ZnONP addition on films. A study of the influence of AgNP and ZnONP on the properties of the film was conducted with a mass ratio of 5, 7, and 9 wt%. The properties of film discussed include transparency, elemental and functional group analysis, WS and WVTR, and antibacterial activity. Figure 4a is a visual display of CS/Ag/OC/ZnO transparency films with the addition of AgNP and ZnONP. The larger the amount of AgNP added, the darker the color of the film. Specifically, the addition of 5% AgNP imparts a golden yellow color to the film. The color becomes darker with the addition of 7% AgNP, and a brownish color appears with the addition of 9% AgNP. Meanwhile, the addition of ZnONP does not affect the color of the film. The color of the resulting film can slightly affect the transparency of the film. This was confirmed by UV–Vis spectra, which did not reveal a remarkable difference in color (Figure 4b). The maximum absorption peak for ZnONP can be observed at 378 nm [33]. SPR of AgNP and ZnONP synthesized by *L.acidissima* leaf extract displayed absorption at 452 and 374 nm, respectively [34].

An analysis of the functional groups and elements in the film was conducted using ATR–FTIR spectroscopy and XRF, respectively (Figures 8). The absorption pattern in Figure 8a does not show remarkable variation from that in Figure 5. The characteristic absorption of montmorillonite is absorption at 1443 cm^{-1}, indicating the Al-O stretching vibrations on Si-O-Al, absorption at a wave number of 1041 cm^{-1} indicates the Si-O stretching vibrations, and absorption at 524 cm^{-1}, indicates the presence of Si-O bending vibrations [35]. The absorption at 3431 cm^{-1} corresponds to the OH group stretching vibration. The band at 1635 cm^{-1} is characteristic of amide I due to the stretching of the carbonyl in CS. The stability of AgNPs may depend on the presence of primary amino groups interacting with the metal surface and the amino groups acting as capping sites [13]. Meanwhile, the absorption of ZnONPs, namely, the band at 896 cm^{-1}, is thought to originate from the weak vibrations of ZnO. The vibrational absorption observed at 500 cm^{-1} was assigned to the Zn–O lattice vibrations in the CS/ZnO nanocomposite [12]. The difference between the uptake on the films, which exhibit varying amounts of AgNP and ZnONP, is that the uptake increases with increasing amounts of ZnONP. The strong interaction between hydroxyl groups and ZnO is evidenced by the presence of a wide hydroxyl group. Absorption in the vibrational bands of 1654 and 1069 cm^{-1} is related to the bending and strain vibration (C–O)–NH2 group [12]. These results agree with the results of characterization using XRF (Figure 8b). The percentage of Ag and Zn elements relatively increased with the increasing amount of AgNP and ZnONP in the film, respectively.

Important film performance tests for food packaging applications include the solubility and WVTR tests. Figure 9 shows the WS and WVTR of the CS/Ag/OC/ZnO film with the addition of AgNP and ZnONP. Food packaging is expected to have a small WS value. The smallest WS value from the study of variations in the amount of addition of AgNP and ZnONP was in the Ag9-ZnO9 sample (0.69 ± 0.1%). The plastic solubility test standard in water (ASTM D570-98 international standard) states that polypropylene plastic has a solubility of 0.1%. However, the solubility properties of CS-based bionanocomposite films were lower than the standard values. The amount of plasticizer concentration added can affect the solubility value of CS-based films [36].

In addition to WS, the WVTR is important for food packaging because the circulation of water vapor from food to the environment is essential [1]. The WVTR value in Figure 9 shows similar values for each sample. The range of WVTR values obtained was 0.25–0.30 g/m^2h. The International Plastic Network summarizes WVTR data for several types of plastics with different polymer types. The WVTR value in this study corresponds to the standard WVTR value for polypropylene (PP)-based plastic, which is 0.2 g/m^2h. The range of WVTR values in this study is slightly higher than the standard value and there are no prominent values, so it can be said that all the variations in the samples are relatively uniform.

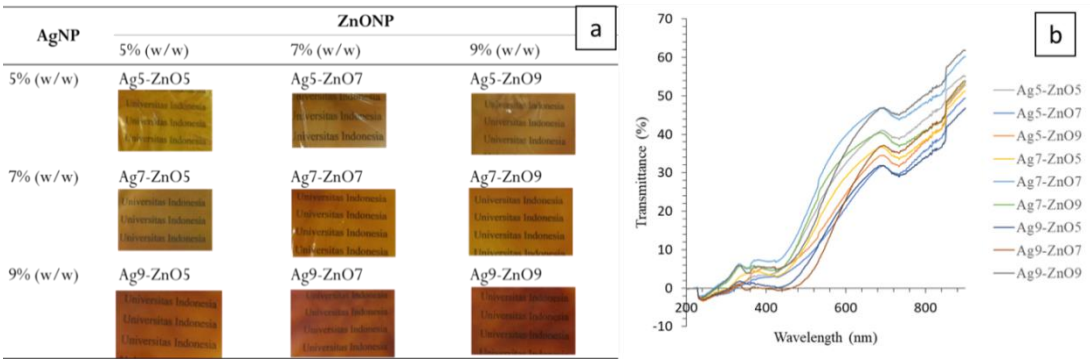

Figure 7. Visual Appearance for the Transparency (a) and Light Transmission Spectra of the CS/Ag/OC/ZnO Film (b) with the Addition of AgNP and ZnONP

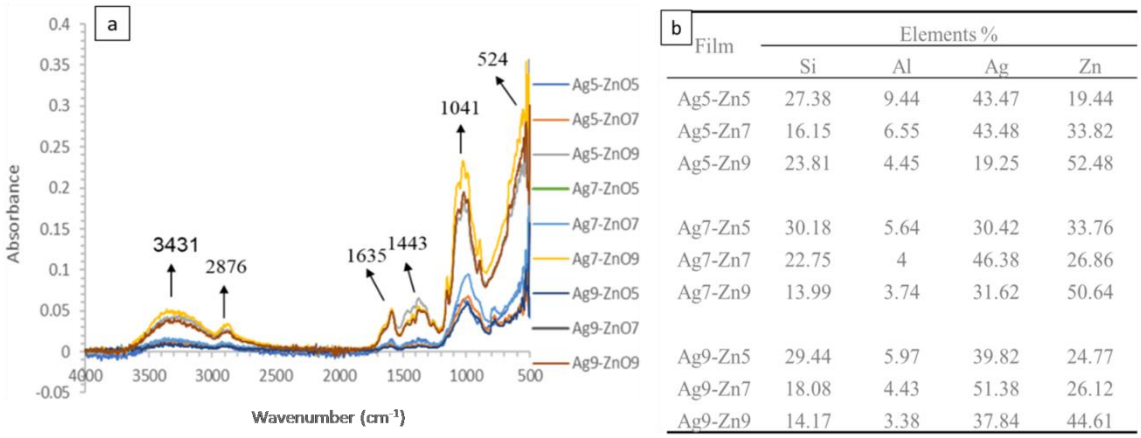

b

Film	Elements %			
	Si	Al	Ag	Zn
Ag5-Zn5	27.38	9.44	43.47	19.44
Ag5-Zn7	16.15	6.55	43.48	33.82
Ag5-Zn9	23.81	4.45	19.25	52.48
Ag7-Zn5	30.18	5.64	30.42	33.76
Ag7-Zn7	22.75	4	46.38	26.86
Ag7-Zn9	13.99	3.74	31.62	50.64
Ag9-Zn5	29.44	5.97	39.82	24.77
Ag9-Zn7	18.08	4.43	51.38	26.12
Ag9-Zn9	14.17	3.38	37.84	44.61

Figure 8. ATR–FTIR Spectra (a) and XRF Characterization Results of the CS/Ag/OC/ZnO Film (b) with the Addition of AgNP and ZnONP

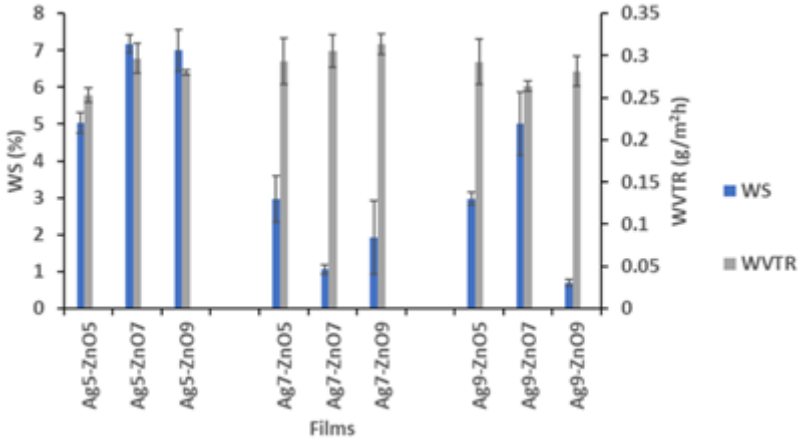

Figure 9. WS and WVTR of the CS/Ag/OC/ZnO Film with the Addition of AgNP and ZnONP

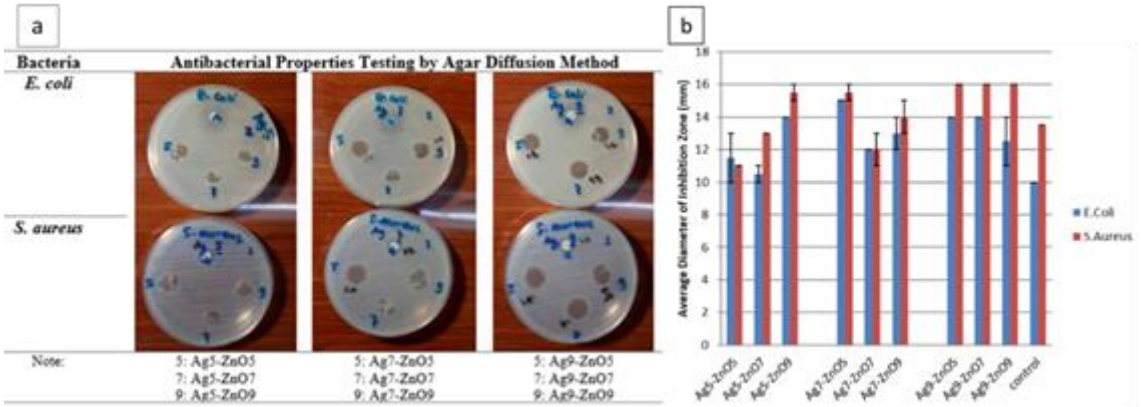

Figure 10. Antibacterial Activities of the CS/Ag/OC/ZnO Film with the Addition of AgNP and ZnONP Against Bacteria (a) and Graphs of the Average Diameter of Inhibition Zone Against Bacteria (b)

The effectiveness of AgNP and ZnONP as antibacterial agents dispersed in the CS matrix was tested with two types of test bacteria, namely *Staphylococcus aureus* (Gram-positive) and *Escherichia coli* (Gram-negative). Both are common pathogenic bacteria in humans. One of the differences between the two is in the membrane: *S. aureus* bacteria only have a single plasma membrane surrounded by peptidoglycan, while *E. coli* bacteria have a double membrane, namely, the plasma membrane covered by a permeable outer membrane.

This antibacterial test used the antibiotic erythromycin as a control for *E. coli* bacteria, while vancomycin was the control for *S. aureus* bacteria. Erythromycin is a type of antibiotic that can inhibit protein synthesis, while vancomycin is a type that can interfere with the synthesis of bacterial cell walls. The antibiotic vancomycin is active against Gram-positive bacteria and is only indicated for infections caused by *S. aureus* bacteria.

The relative inhibition zone increased with an increasing number of Ag and ZnO nanoparticles. Thus, the Ag9-ZnO9 sample has the largest inhibition zone. Although this sample has the smallest *E. coli* inhibition zone value among the variations in the amount of Ag in 9 wt% ZnO, the standard deviation value is high so that it can be uniform with other inhibition zone values.

The amount of Ag^+ ion production is affected by the size and shape of the AgNPs. The Ostwald-Freundlich equation can theoretically explain this phenomenon. According to this equation, the surface area or particle size of AgNPs can affect the release of Ag^+ ions. Thus, the way to reduce aggregation and increase AgNP activity is to overcome it by using capping agents, which effectively modify the surface of AgNPs. In addition to the inherent properties of AgNPs, the surrounding media, such as the presence of organic or inorganic compounds, and the acid-base environment in the AgNP environment can affect the release of Ag^+ ions [2].

Gram-positive pathogens consist of a very thick cell wall composed of various peptidoglycan sheaths, thus serving as a barrier to the permeation of Ag^+ ions through the cytoplasmic membrane. However, most gram-negative pathogens consist of only one peptidoglycan coat, so Ag^+ ions easily enter the cytoplasm and cause cell death.

The proposed antibacterial mechanism of ZnONP includes direct interaction between ZnONP and bacterial cells affecting cell membrane permeability after membrane disorganization and changing protein structure. The proton motive force and absorption of dissolved zinc ions encourage the entry of ZnONP and cause oxidative stress in bacterial cells, which then form reactive oxygen species (ROS). High reactivity and oxidizing properties can increase the toxicity of ROS to bacteria, including damage to cellular components such as lipids, DNA, and proteins, due to their incorporation into the membrane of the bacterial cell. Another mechanism, ZnONP, can also activate respiratory enzymes, causing inadequate mitochondrial function and inhibition of cell metabolism and flow of cytoplasmic contents, which ultimately leads to the inhibition of cell growth and/or bacterial cell death [37].

Conclusions

The silver/zinc oxide nanoparticles/organoclay–reinforced CS biocomposites (CS/Ag/OC/ZnO) were prepared and well characterized. The AgNPs were successfully synthesized using local CS as a reducing agent and capping agent. The addition of 9 wt% AgNP and ZnONP into the CS/Ag/OC/ZnO film was successful and provided antibacterial activity on *E. coli* and *S. aureus.* Therefore, the structural, mechanical, optical, and antibacterial properties of CS/Ag/OC/ZnO films have the potential to be used in food packaging applications.

Acknowledgement

This work was supported by the Directorate of Research and Development, Universitas Indonesia (Doctoral International Indexed Publications: NKB-616/UN2.RST/HKP.05.00/2020) and Indonesian Ministry of Education and Culture for granting Domestic Postgraduate Education Scholarships.

Author Contributions

Lisna Junaeni Muiz: writing-original draft and visualization. Ariadne Lakshmidevi Juwono: supervision and writing-review & editing. Zulkarnaen Paputungan: assist in the discussion of material preparation and writing-review. Yuni Krisyuningsih Krisnandi: methodology, conceptualization, funding acquisition, writing-review & editing, and supervision.

References

[1] Huang, Y., Mei, L., Chen, X., Wang, Q. 2018. Recent developments in food packaging based on nanomaterials. Nanomaterials. 8(10): 830, https://doi.org/10.3390/nano8100830.

[2] Ahmad, S.A., Das, S.S., Khatoon, A., Ansari, M.T., Afzal, M., Hasnain, M.S., *et al*. 2020. Bactericidal activity of silver nanoparticles: A mechanistic review. Mater. Sci. Energy Technol. 3: 756–769, https://doi.org/10.1016/j.mset.2020.09.002.

[3] Badiger, P.P.M., Patil, P.M., Badiger, M.V., Patel, P.R., Gadgil, B.S.T., Pandit, A., Bohara, R.A. 2020. Biofilm formation to inhibition: Role of zinc oxide-based nanoparticles. Mater. Sci. Eng. C. 108: 110319, https://doi.org/10.1016/j.msec.2019.110319.

[4] Sharma, V.K., Yngard, R.A., Lin, Y. 2009. Silver nanoparticles: Green synthesis and their antimicrobial activities. Adv. Coll. Inter. Sci. 145(1–2): 83–96, https://doi.org/10.1016/j.cis.2008.09.002.

[5] Zain, N.M., Stapley, A.G.F., Shama, G. 2014. Green synthesis of silver and copper nanoparticles using ascorbic acid and chitosan for antimicrobial applications. Carbohydr. Polym. 112: 195–202, https://doi.org/10.1016/j.carbpol.2014.05.081.

[6] Wongpreecha, J., Polpanich, D., Suteewong, T., Kaewsaneha, C., Tangboriboonrat, P. 2018. One-pot, large-scale green synthesis of silver nanoparticles-chitosan with enhanced antibacterial activity and low cytotoxicity. Carbohydrate Polym. 199: 641–648, https://doi.org/10.1016/j.carbpol.2018.07.039.

[7] Fetouh, H.A., Hefnawy, A., Attia, A.M., Ali, E. 2020. Facile and low-cost green synthesis of eco-friendly chitosan-silver nanocomposite as novel and promising corrosion inhibitor for mild steel in chilled water circuits. J. Mol. Liq. 319: 114355, https://doi.org/10.1016/j.molliq.2020.114355.

[8] Affes, S., Maalej, H., Aranaz, I., Kchaou, H., Acosta, N., Heras, Á., *et al*. 2020. Controlled size green synthesis of bioactive silver nanoparticles assisted by chitosan and its derivatives and their application in biofilm preparation. Carbohyd. Polym. 236: 116063, https://doi.org/10.1016/j.carbpol.2020.116063.

[9] Gabriel, J.S., Gonzaga, V.A.M., Poli, A.L., Schmitt, C.C. 2017. Photochemical synthesis of silver nanoparticles on chitosans/montmorillonite nanocomposite films and antibacterial activity. Carbohyd. Polym. 171: 202–210, https://doi.org/10.1016/j.carbpol.2017.05.021.

[10] Zahedi, Y., Achachlouei, B.F., Yousefi, A.R. 2018. Physical and mechanical properties of hybrid montmorillonite/zinc oxide reinforced carboxymethyl cellulose nanocomposites. Int. J. Biol. Macromol. 108: 863–873, https://doi.org/10.1016/j.ijbiomac.2017.10.185.

[11] Nouri, A. Yaraki, M.T., Ghorbanpour, M., Agarwal, S., Gupta, V.K. 2018. Enhanced antibacterial effect of chitosan film using montmorillonite/CuO nanocomposite. Int. J. Biol. Macromol. 109: 1219–1231, https://doi.org/10.1016/j.ijbiomac.2017.11.119.

[12] Magesh, G., Bhoopathi, G., Nithya, N., Arun, A.P., Kumar, E.R. 2018. Tuning effect of polysaccharide Chitosan on structural, morphological, optical and photoluminescence properties of ZnO nanoparticles. Superlattice. Microstr. 117: 36–45, https://doi.org/10.1016/j.spmi.2018.03.003.

[13] Kalaivani, R., Maruthupandy, M., Muneeswaran, T., Beevi, A.H., Anand, M., Ramakritinan, C.M., *et al*. 2018. Synthesis of chitosan mediated silver nanoparticles (Ag NPs) for potential antimicrobial applications. Front. Lab. Med. 2(1): 30–35, https://doi.org/10.1016/j.flm.2018.04.002.

[14] Visurraga, J.D., Melendrez, M.F., Garcia, A., Paulraj, M., Cardenas, G. 2010. Semitransparent chitosan-TiO_2 nanotubes composite film for food package applications. J. Appl. Polym. Sci. 116(6): 3503–3515, https://doi.org/10.1002/app.31881.

[15] Kumar, M., Panjagari, N.R., Kanade, P.P., Singh, A.K., Badola, R., Ganguly, S., *et al*. 2018. Sodium caseinate-starch-modified montmorillonite based biodegradable film: Laboratory food extruder assisted exfoliation and characterization. Food Packag. Shelf Life. 15: 17–27, https://doi.org/10.1016/j.fpsl.2017.12.008.

[16] Bhat, V.G., Narasagoudr, S.S., Masti, S.P., Chougale, R.B., Shanbhag, Y. 2021. Hydroxy citric acid cross-linked chitosan/guar gum/poly(vinyl alcohol) active films for food packaging applications. Int. J. Biol. Macromol. 177: 166–175, https://doi.org/10.1016/j.ijbiomac.2021.02.109.

[17] Helmiyati, H., Hidayat, Z.S.Z., Sitanggang, I.F.R., Liftyawati, D. 2021. Antimicrobial packaging of ZnO–Nps infused into CMC–PVA nanocomposite films effectively enhances the physicochemical properties. Polym. Test. 104: 107412, https://doi.org/10.1016/j.polymertesting.2021.107412.

[18] Sarwar, M.S., Niazi, M.B.K., Jahan, Z., Ahmad, T., Hussain, A. 2018. Preparation and characterization of PVA/nanocellulose/Ag nanocomposite films for antimicrobial food packaging. Carbohyd. Polym. 184: 453–464, https://doi.org/10.1016/j.carbpol.2017.12.068.

[19] Alrin, E., Tjampakasari, C.R., Krisnandi, Y.K. 2022. Metal-organic framework derived ZnO/porous carbon−13X zeolite composite modified with chitosan and silver nanoparticles as versatile antibacterial agent. Inorg Chem. Commun. 144: 109943, https://doi.org/10.1016/j.inoche.2022.109943.

[20] Reicha, F.M., Sarhan, A., Hamid, M.I.A., El-Sherbiny, I.M. 2012. Preparation of silver nanoparticles in the presence of chitosan by electrochemical method. Carbohyd. Polym. 89(1): 236–244, https://doi.org/10.1016/j.carbpol.2012.03.002.

[21] Austin, L.A., MacKey, M.A., Dreaden, E.C., El-Sayed, M.A. 2014. The optical, photothermal, and facile surface chemical properties of gold and silver nanoparticles in biodiagnostics, therapy, and drug delivery. Arch. Toxicol. 88: 1391–1417, https://doi.org/10.1007/s00204-014-1245-3.

[22] Nate, Z., Moloto, M.J., Mubiayi, P.K., Sibiya, P.N. 2018. Green synthesis of chitosan capped silver nanoparticles and their antimicrobial activity. MRS Adv. 3: 2505–2517, https://doi.org/10.1557/adv.2018.368.

[23] Su, L., Huang, J., Li, H., Pan, Y., Zhu, B., Zhao, Y., *et al*. 2021. Chitosan-riboflavin composite film based on photodynamic inactivation technology for antibacterial food packaging. Int. J. Biol. Macromol. 172: 231–240, https://doi.org/10.1016/j.ijbiomac.2021.01.056.

[24] Ulyarti, U., Lavlinesia, L., Surhaini, S., Siregar, N., Tomara, A., Lisani, L., *et al*. 2021. Development of yam-starch-based bioplastics with the addition of chitosan and clove oil. Makara J. Sci. 25(2): 91–97, https://doi.org/10.7454/mss.v25i2.1155.

[25] Juwono, A., Edward, G. 2006. A study of clay-epoxy nanocomposites consisting of unmodified clay and organo clay. Makara J. Sci. 10(1): 6–12.

[26] Pradisty, N.A., Sihombing R., Howe, R.F., Krisnandi, Y.K. 2017. Fe (III) oxide-modified indonesian bentonite for catalytic photodegradation of phenol in water. Makara J. Sci. 21(1): 25–33, https://doi.org/10.7454/mss.v21i1.7534.

[27] Khodashenas, B., Ghorbani, H.R. 2019. Synthesis of silver nanoparticles with different shapes. Arab. J.

Chem. 12(8): 1823–1838, https://doi.org/10.1016/j.arabjc.2014.12.014.
[28] Zhang, L., Wang, H., Jin, C., Zhang, R., Li, L., Li, X., *et al*. 2017. Sodium lactate loaded chitosan-polyvinyl alcohol/montmorillonite composite film towards active food packaging. Innov. Food Sci. Emerg. Technol. 42: 101–108, https://doi.org/10.1016/j.ifset.2017.06.007.
[29] Saha, N.R., Sarkar, G., Roy, I., Bhattacharyya, A., Rana, D., Dhanarajan, G., *et al*. 2016. Nanocomposite films based on cellulose acetate/polyethylene glycol/modified montmorillonite as nontoxic active packaging material. RSC Adv. 6: 92569–92578, https://doi.org/10.1039/c6ra17300d.
[30] Zhao, J., Wei, F., Xu, W., Han, X. 2019. Enhanced antibacterial performance of gelatin/chitosan film containing capsaicin loaded MOFs for food packaging. Appl. Surf. Sci. 510: 145418, https://doi.org/10.1016/j.apsusc.2020.145418.
[31] Mousavi, S.M., Behbudi, G., Gholami, A., Hashemi, S.A., Nejad, Z. M., Bahrani, S., *et al*. 2022. Shape-controlled synthesis of zinc nanostructures mediating macromolecules for biomedical applications. Biomater. Res. 26: 4, https://doi.org/10.1186/s40824-022-00252-y.
[32] Block, K.A., Trusiak, A., Katz, A., Alimova, A., Wei, H., Gottlieb, P., *et al*. 2015. Exfoliation and intercalation of montmorillonite by small peptides. Appl. Clay Sci. 107: 173–181, https://doi.org/10.1016/j.clay.2015.01.021.
[33] Muiz, L.J., Juwono, A.L., Krisnandi,Y.K. 2022. A review: Silver-zinc oxide nanoparticles-organoclay-reinforced chitosan bionanocomposites for food packaging. Open Chem. 20(1): 1155–1170, https://doi.org/10.1515/chem-2022-0224.
[34] El-saied, H.A., Ibrahim, A.M. 2020. Effective fabrication and characterization of eco-friendly nano chitosan capped zinc oxide nanoparticles for effective marine fouling inhibition. J. Environ. Chem. Eng. 8(4): 103949, https://doi.org/10.1016/j.jece.2020.103949.
[35] Patil, B.N., Taranath, T.C. 2018. *Limonia acidissima* L. leaf mediated synthesis of silver and zinc oxide nanoparticles and their antibacterial activities. Microb. Pathogenesis. 115: 227–232, https://doi.org/10.1016/j.micpath.2017.12.035.
[36] Paluszkiewicz, C., Stodolak, E., Hasik M., Blazewicz, M. 2011. FT-IR study of montmorillonite-chitosan nanocomposite materials. Spectrochim. Acta A. 79(4): 784–788, https://doi.org/10.1016/j.saa.2010.0 8.053.
[37] Costa, S.M., Ferreira, D.P., Teixeira, P., Ballesteros, L.F., Teixeira, J.A., Fangueiro, R. 2021. Active natural-based films for food packaging applications: The combined effect of chitosan and nanocellulose. Int. J. Biol. Macromol. 177: 241–251, https://doi.org/10.1016/j.ijbiomac.2021.02.105.